Comput Mech (2009) 43:545–557
DOI 10.1007/s00466-008-0329-4

ORIGINAL PAPER

The role of weakly imposed Dirichlet boundary conditions for numerically stable computations of swelling phenomena

W. Ehlers · A. Acartürk

Received: 11 May 2007 / Accepted: 3 August 2008 / Published online: 27 August 2008

Abstract It is still a challenge to model swelling phenomena occurring in charged hydrated porous media. This is not only due to the overall complexity of the model but also to the fact that boundary conditions occur, which depend on internal variables. In the present contribution, a multi-component model based on the Theory of Porous Media (TPM) is presented. The advantage of this model is that it is thermodynamically consistent and it consists of only three primary variables. As a result of the boundary conditions depending on internal variables, the numerical treatment within the finite element method (FEM) by use of the mixed finite element scheme reveals artificial oscillations in the numerical results. To overcome these oscillations, we propose to fulfil boundary conditions weakly.

Keywords TPM · Swelling porous media · Charged hydrated materials · Finite deformations · Weakly fulfilled *Dirichlet* boundary conditions

1 Introduction

The aim of this contribution is to model swelling phenomena which occur in charged hydrated media such as active soil or soft biological tissue. These materials have a multiphasic porous microstructure including a charged solid matrix and an interstitial fluid. In particular, the solid matrix of, e.g., active clay is composed of negatively charged silicate platelets, while the matrix of soft biological tissue such as articular cartilage or intervertebral discs is composed of collagen fibres and proteoglycan aggregates (PGA) with adhering fixed charges. Although inhomogeneities and anisotropies may occur in reality, especially in the investigation of biological tissue, the present article is restricted to homogeneous and isotropic materials; for anisotropic and non-homogeneous conditions, cf. [14]. Furthermore, the interstitial fluid itself is a solution composed of multiple components, namely, the liquid solvent and the positively and negatively charged ions (cations and anions) of a dissolved salt. For a more precise description of these constituents, cf. [17,35].

As one can imagine, there are many complex mechanical and electrochemical effects like deformation, convection, diffusion and osmosis as well as electrical currents interacting with each other. The continuum mechanical description of materials with these properties leads to a complex nonlinear system of strongly coupled partial differential equations (PDE), which have to be solved by numerical methods such as the Finite Element Method (FEM) within the mixed finite element scheme. Furthermore, it can be shown that it is sufficient to proceed from three primary variables, the solid deformation, the overall pore-fluid pressure and the molar concentration of the cations dissolved in the pore-fluid solution. Correspondingly, the governing PDEs are the momentum balance of the overall aggregate as well as the volume balance of the overall pore fluid and the cation concentration balance.

During the numerical solution of initial boundary-value problems governing swelling processes, where the swelling medium is surrounded by an external solution interacting with both the swelling solid and its pore-fluid content, it occurs that non-standard boundary conditions have to be applied, where, at the internal boundary, the external values cannot simply be matched through the degrees of freedoms included in the set-up functions of the primary variables in

W. Ehlers (✉) · A. Acartürk
Institute of Applied Mechanics (CE), University of Stuttgart,
Pfaffenwaldring 7, 70 569 Stuttgart, Germany
e-mail: ehlers@mechbau.uni-stuttgart.de

A. Acartürk
e-mail: acar@mechbau.uni-stuttgart.de

combination with the constitutive equations of the model. Instead, they additionally depend on internal variables such as the fixed charges concentration of the swelling material given as a function of the solid deformation. This induces a jump of the primary variables across the boundary.

In the literature of swelling media, most of the publications up to now deal with one-dimensional (1-d) models and simulations, cf. [29,33,40] or [21]. For the 1-d case, no numerical problems could be observed. Only in case of higher dimensional simulations, the deformation-dependent boundary conditions lead to numerical instabilities, since the error made at each boundary node by use of a non-matching fixed charges concentration, such as the value of the last accepted time step, yields gradients along the boundary, which in turn sum up to spurious oscillations. These instabilities have also been observed by other authors, cf. [39]. In their publication, [39] solved the problem of numerical instabilities in a two-dimensional (2-d), axisymmetric model of the intervertebral disc by means of a least squares method, where, at the boundary, the error of both the concentration and the pressure weighted by certain factors was minimised. Other possibilities, which we have used to overcome the numerical instabilities, consist of taking the value of the respective internal variable from an inner element layer, cf. [1], or of averaging the value over several boundary nodes. These solutions are first attempts to isolate the problem and need no additional memory and numerical cost. A further possibility to describe swelling behaviour is to take the chemical potentials of the fluid components as primary variables instead of concentrations, cf. [20,32,44]. While the obvious advantage of the latter approach is that the boundary conditions are continuous, the disadvantage is the higher number of degrees of freedom, which in turn results in higher memory requirements and longer simulation times. Finally, in [14,15], a model based on the Lanir assumption [31] is discussed. Therein, it is assumed that only very small concentration variations occur, which in turn lead to an immediate chemical equilibrium. As a result, the cation concentration is taken as a material parameter and the set of primary variables reduces to the solid deformation and the fluid pressure.

In frame of the full swelling model computed at shortest simulation times without any model reduction, it appears that including the molar concentration of the cations as a primary variable instead of chemical potentials is the most reasonable choice. However, the oscillation problem occurring as a result of deformation-dependent boundary conditions has to be overcome. This leads to the field of free surface problems or of fluid–structure interactions (FSI), where boundary conditions similar to those described above are well known. For example, considering the *Lagrange*an description, which is also used for the solid skeleton in the present contribution, the mesh of a free surface problem moves with the deforming fluid. The successful solution of these problems range back to [37] who implemented the additional boundary condition at the free surface into the weak formulation of the *Navier–Stokes* equation, cf. also [23,36,43]. Following this idea, we introduce a continuum mechanical multi-field and multi-physical model, where two of the three essential boundary conditions involved depending on internal and primary variables are included into the weak formulation of the overall problem. Thus, these boundary conditions are imposed weakly.

The present contribution starts in Sect. 2 with a brief discussion of the multiphase formulation of the TPM and the underlying constitutive approach, where a consistent swelling model with only three primary variables is derived. In Sect. 3 , a numerically effective and consistent method to account for the solution of numerical problems resulting from deformation-dependent boundary conditions is presented. This method proceeds from the inclusion of weakly imposed *Dirichlet* boundary conditions into the mixed finite element formulation by use of a penalty-like method. Finally, the model is validated in Sect. 4 by numerical computations, where the capability and the stability of the model are shown via a 2-d simulation of a free swelling hydrogel block exhibiting finite deformations.

2 Multiphase formulation

2.1 Basics

Proceeding from a continuum-mechanical approach, the theory of porous media (TPM) [3,4,6,10,11,34] is used to describe materials with a multiphasic composition of the microstructure. The TPM is based on the well-known theory of mixtures (TM) [5] extended by the concept of volume fractions such that the constituents and their properties are 'smeared' over the spatial domain under consideration. Following this, the TPM can be understood as the result of either a real or a virtual averaging procedure over representative elementary volumes (REV), cf. Fig. 1. In any case, one obtains the most effective possibility to describe materials with a multiphasic microstructural composition of components.

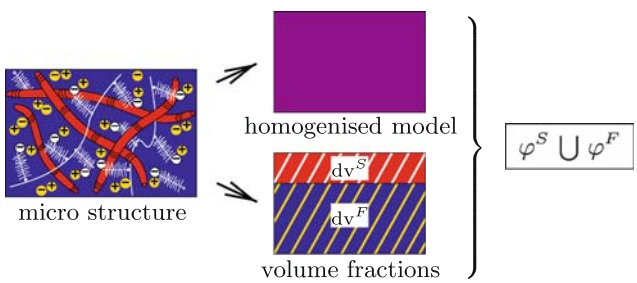

Fig. 1 Micro structure and macroscopic model

The overall medium φ under consideration is composed of multiple miscible and immiscible constituents φ^α. In particular, we start from a biphasic medium of immiscible constituents modelled by the TPM: the charged solid matrix ($\alpha = S$) including the mass- and volume-free fixed charges φ^{fc} adhering to the solid material and the charged fluid ($\alpha = F$). Moreover, since the fluid itself represents a mixture of three miscible components φ^β, namely, the liquid solvent ($\beta = L$) and the cations ($\beta = +$) and anions ($\beta = -$) of a dissolved salt, the charged fluid is modelled in the framework of the TM.

2.2 Constituents, volume fractions, densities and concentrations

Proceeding from the TM or the TPM, the constituents of the overall medium can be identified by their volume fractions n^α, which relate the local volume $\mathrm{d}v^\alpha$ of the constituent φ^α to the local bulk volume $\mathrm{d}v$ of φ ($n^\alpha = \mathrm{d}v^\alpha/\mathrm{d}v$). Assuming that there is no vacant space in the domain, the saturation condition reads

$$\sum_{\alpha=S,F} n^\alpha = n^S + n^F = 1, \quad \text{where} \quad n^F = \sum_{\beta=L,+,-} n^\beta = n^L + n^+ + n^-. \tag{1}$$

Note in passing that the saturation condition is a constraint to the composition of the overall model and has thus to be included in the constitutive equations, cf. [11]. Introducing the volume fractions, the individual components can be described by two densities, the partial and the effective one. The former relates the local mass $\mathrm{d}m^\alpha$ of the individual constituents φ^α ($\alpha = S, L, +, -$) to the local bulk volume ($\rho^\alpha = \mathrm{d}m^\alpha/\mathrm{d}v$), whereas the latter relates the same mass to the local constituent volume ($\rho^{\alpha R} = \mathrm{d}m^\alpha/\mathrm{d}v^\alpha$). Both densities are related to each other by

$$\rho^\alpha = n^\alpha \rho^{\alpha R}. \tag{2}$$

Moreover, the amount of matter of the components φ^β constituting the pore fluid φ^F is given by the molar concentration

$$c_m^\beta = \frac{\mathrm{d}n_m^\beta}{\mathrm{d}v^F} \tag{3}$$

defined as the ratio of the local number of moles $\mathrm{d}n_m^\beta$ of the component φ^β over the local bulk fluid volume $\mathrm{d}v^F$. The partial density ρ^β of the fluid component is related to its molar concentration via

$$\rho^\beta = n^F \rho_F^\beta = n^F c_m^\beta M_m^\beta. \tag{4}$$

In the above relation, M_m^β denotes the molar mass of φ^β and ρ_F^β the corresponding partial density with respect to the fluid volume ($\rho_F^\beta = \mathrm{d}m^\beta/\mathrm{d}v^F$). Finally, there exists a further restriction to the behaviour of the overall model. This restriction, the electrostatic counterpart of the saturation condition, is the electroneutrality condition:

$$\begin{aligned} z^+ c_m^+ + z^- c_m^- + z^{fc} c_m^{fc} &= 0, \\ z^+ \bar{c}_m^+ + z^- \bar{c}_m^- &= 0. \end{aligned} \tag{5}$$

Equation $(5)_1$ states that there is neither a charge separation within the overall medium given by the solid matrix and the internal pore-fluid mixture nor within the external solution, cf. $(5)_2$. Using the valences $z^+ = 1$ and $z^- = -1$ of the ions of a monovalent salt such as $\mathsf{Na^+Cl^-}$, the electroneutrality condition of the external solution reveals that the concentrations of the ions therein, denoted by a bar, are equal and can be addressed by only one variable, the cation concentration $\bar{c}_m^+$. Thus, the external electroneutrality condition reads

$$z^+ \bar{c}_m^+ + z^- \bar{c}_m^- = 0 \longrightarrow \bar{c}_m^- = \bar{c}_m^+ =: \bar{c}_m. \tag{6}$$

Concerning the internal solution and considering that the solid matrix is negatively charged, the cation concentration c_m^+ is taken as a primary variable. This is convenient in so far as in case of an infinitely dilute external solution, the anion concentration within the overall medium tends to zero, thus inducing numerical difficulties. Inserting the valences of the ions and the fixed charges with $z^{fc} = -1$, it is obvious that the anion concentration c_m^- can be given as a function of c_m^+ and the concentration c_m^{fc} of the fixed charges, cf. [27,30]:

$$z^+ c_m^+ + z^- c_m^- + z^{fc} c_m^{fc} = 0 \longrightarrow \begin{cases} c_m^+ =: c_m \\ c_m^- = c_m - c_m^{fc} \end{cases}. \tag{7}$$

2.3 Kinematics

As depicted in Fig. 1, the continuum mechanical approach of the TPM proceeds from the assumption that all the constituents are smeared over the REV in the sense of superimposed and interacting continua, cf. Fig. 2.
Furthermore, in the current configuration at time t, each spatial point $\mathbf{x}$ is simultaneously occupied by all constituents

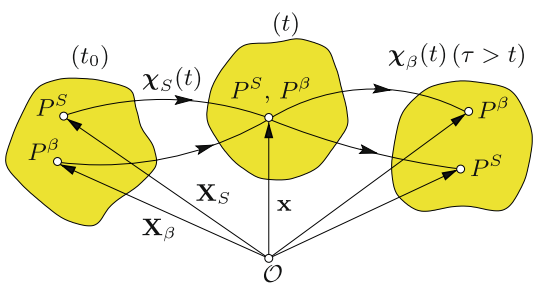

Fig. 2 Kinematics of an aggregate with solid phase φ^S and fluid components φ^β

φ^α stemming from different initial positions $\mathbf{X}_\alpha$ at $t = t_0$. Following this, each constituent follows its individual motion function $\boldsymbol{\chi}_\alpha$ and, therefore, has its own *Lagrange*an velocity:

$$\mathbf{x} = \boldsymbol{\chi}_\alpha(\mathbf{X}_\alpha, t), \quad \overset{'}{\mathbf{x}}_\alpha = \frac{\mathrm{d}\boldsymbol{\chi}_\alpha(\mathbf{X}_\alpha, t)}{\mathrm{d}t}. \tag{8}$$

Therein, $(\cdot)'_\alpha$ denotes the material time derivative following the motion of φ^α. The motion of the solid phase is expressed within a *Lagrange*an representation by the displacement vector

$$\mathbf{u}_S = \mathbf{x} - \mathbf{X}_S, \tag{9}$$

whereas the motion of the interstitial fluid φ^F and its components φ^β is given in an *Euler*ian setting by the seepage velocities

$$\mathbf{w}_F = \overset{'}{\mathbf{x}}_F - \overset{'}{\mathbf{x}}_S \quad \text{and} \quad \mathbf{w}_\beta = \overset{'}{\mathbf{x}}_\beta - \overset{'}{\mathbf{x}}_S\,. \tag{10}$$

Therein, the seepage velocity $\mathbf{w}_F$ describes the motion of the overall fluid, while $\mathbf{w}_\beta$ is the velocity of the fluid components relative to the deforming skeleton. Combining Eqs. (8) and (9), the solid deformation gradient yields

$$\mathbf{F}_S := \frac{\partial \mathbf{x}}{\partial \mathbf{X}_S} = \mathbf{I} + \mathrm{Grad}_S\, \mathbf{u}_S. \tag{11}$$

Therein, the operator $\mathrm{Grad}_S\,(\cdot) = \partial(\cdot)/\partial\mathbf{X}_S$ denotes the partial derivative of $(\cdot)$ taken with respect to the solid reference position.

2.4 Balance relations

Proceeding from quasi-static processes ($\overset{''}{\mathbf{x}}_\alpha \equiv \mathbf{0}$) and assuming materially incompressible constituents ($\rho^{\alpha R} \equiv$ const.) incapable of mass exchanges ($\hat{\rho}^\alpha \equiv 0$), one obtains a model governed by the volume and momentum balances of the constituents φ^α and the concentration balances of the fluid components φ^β, cf. [16]:

$$\begin{aligned} &(n^\alpha)'_\alpha + n^\alpha \,\mathrm{div}\, \overset{'}{\mathbf{x}}_\alpha = 0, \\ &(n^F c_m^\beta)'_\beta + n^F c_m^\beta \,\mathrm{div}\, \overset{'}{\mathbf{x}}_\beta = 0, \\ &\mathrm{div}\, \mathbf{T}^\alpha + \rho^\alpha \mathbf{b} + \hat{\mathbf{p}}^\alpha = \mathbf{0}. \end{aligned} \tag{12}$$

Therein, $\mathrm{div}(\cdot)$ denotes the divergence operator corresponding to $\mathrm{grad}(\cdot) = \partial(\cdot)/\partial\mathbf{x}$, $\mathbf{T}^\alpha$ is the *Cauchy* stress tensor, $\rho^\alpha\mathbf{b}$ is the volume force, and $\hat{\mathbf{p}}^\alpha$ is the interaction force (direct momentum production) between the constituents with the constraint $\sum_\alpha \hat{\mathbf{p}}^\alpha = \mathbf{0}$. With the knowledge of the deformation gradient (11), the solid volume balance $(12)_1$ can be time-integrated analytically. In addition, a volume balance for the fixed charges is introduced and, since these charges are attached to the solid matrix, thus following the solid motion, this balance can be integrated analytically, as well. The result is one equation for the solid volume fraction n^S, the solidity, and one for the concentration of the fixed charges:

$$\begin{aligned} n^S &= n^S_{0S}(\det \mathbf{F}_S)^{-1}, \\ c_m^{fc} &= n^F_{0S}\, c^{fc}_{m0S}\, (\det \mathbf{F}_S - n^S_{0S})^{-1}. \end{aligned} \tag{13}$$

Note that the values indicated by $(\cdot)_{0S}$ denote the corresponding initial terms at $t = t_0$. Moreover, concerning the components of the overall fluid, it is assumed that $c_m^L \gg \{c_m^+,\, c_m^-\}$ thus including $\overset{'}{\mathbf{x}}_L \approx \overset{'}{\mathbf{x}}_F$ and $c_m^L \approx$ const. Following this, the concentration balance $(12)_2$ of the liquid approximately coincides with the volume balance $(12)_1$ of the overall fluid, which is rearranged such that

$$\mathrm{div}\,[\,(\mathbf{u}_S)'_S + n^F \mathbf{w}_F\,] = 0 \tag{14}$$

represents the saturation constraint. Furthermore, the cation concentration balance $(12)_2$ ($\beta = +$) is rearranged with $c_m^+ = c_m$ by use of the solid volume balance and by expressing the material time derivative with respect to the moving solid skeleton. Thus,

$$n^F (c_m)'_S + c_m \,\mathrm{div}(\mathbf{u}_S)'_S + \mathrm{div}(n^F c_m\, \mathbf{w}_+) = 0. \tag{15}$$

Note in passing that the electroneutrality condition (7) for the internal solution induces that only one of the ion concentration balances is needed. The momentum balance of the overall medium

$$\mathbf{0} = \mathrm{div}\,(\mathbf{T}^S_{E\,mech.} - p\,\mathbf{I}) + \rho\,\mathbf{b} \tag{16}$$

is derived by summing over the momentum balances of φ^S and φ^F and using the effective stress principle as described in [16]. In the above equation, $\mathbf{T}^S_{E\,mech.}$ stands for the purely mechanical part of the solid extra stress discussed later in this contribution, while $\rho\,\mathbf{b}$ with $\rho = \rho^S + \rho^F$ is the volume force acting on the overall medium. Note additionally that the entire pore-fluid pressure p consists of two portions and is defined by the relation

$$p := \mathcal{p} + \pi. \tag{17}$$

Therein, the first term is the *Lagrange*an multiplier $\mathcal{p}$ identified as the hydraulic pressure acting on the saturation constraint of the overall model, while the second term is the osmotic pressure π, cf. also Fig. 3 for the different occurring pressures. Note that $\mathcal{p}$ is obtained from the respective boundary conditions, while π develops from concentration differences.

2.5 Constitutive theory

2.5.1 Solid matrix

It is well known that the solid matrix of swelling materials can undergo large deformations. For example, when drilling for oil through a layer of active clay, this layer may swell such that the drill gets stuck in the bore hole. To be able

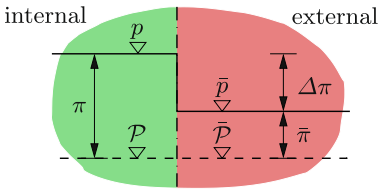

Fig. 3 Pressure evolution across the boundary. It can be seen that the difference between the pressures in both regions is the osmotic pressure difference $\Delta\pi$

to simulate these large elastic deformations accurately, the solid matrix is modelled by a modified Neo-*Hooke*an material law accounting for non-linear deformations as well as for the so-called compression point. The compression point exhibits a specific characteristic of porous materials with a materially incompressible solid skeleton. This point is reached, if the whole fluid is pressed out of the medium such that only the solid is remaining. Recalling that the solid is incompressible, further compression would lead to infinite stresses. Following this, we proceed from the non-linear elasticity law proposed by [12], which is based on an extension of the Neo-*Hooke*an model towards finite volumetric strains including the compression point mentioned before:

$$\boldsymbol{\tau}^S_{E\,mech.} := \mu^S(\mathbf{B}_S - \mathbf{I}) + \lambda^S (1 - n^S_{0S})^2 \left(\frac{\det \mathbf{F}_S}{1 - n^S_{0S}} - \frac{\det \mathbf{F}_S}{\det \mathbf{F}_S - n^S_{0S}} \right) \mathbf{I}. \quad (18)$$

In the above relation, the *Kirchhoff* extra stress tensor $\boldsymbol{\tau}^S_{E\,mech.}$ is related to the *Cauchy* stress $\mathbf{T}^S_{E\,mech.}$ via $\boldsymbol{\tau}^S_{E\,mech.} = \det \mathbf{F}_S\, \mathbf{T}^S_{E\,mech.}$, μ^S and λ^S are the *Lamé* constants and $\mathbf{B}_S = \mathbf{F}_S\, \mathbf{F}_S^T$ stands for the left *Cauchy–Green* deformation tensor.

2.5.2 Fluid flow and ion diffusion

In addition, relations for the fluid and the ion movement are needed. These equations can then be inserted into the corresponding balance relations, namely, the volume balance (14) of the overall fluid and the concentration balance (15) of the cations.

Firstly, to derive an equation describing the fluid flow, the momentum production and the partial stress of the overall fluid are inserted into the fluid balance of momentum, cf. [16]. Following this, one obtains after some rearrangements an extended *Darcy*-type equation:

$$n^F \mathbf{w}_F = -\frac{k^F}{\gamma^{FR}} \Big[\operatorname{grad} \mathcal{P} - \rho^{FR}\, \mathbf{b} + \frac{2c_m - c_m^{fc}}{\sum_\beta c_m^\beta} R\theta \operatorname{grad}(2c_m - c_m^{fc}) - z^{fc} c_m^{fc} \operatorname{grad} \mathcal{E} \Big]. \quad (19)$$

The same procedure applied to the momentum balance of the ions φ^γ ($\gamma = +, -$) leads to the extended *Fick*-type equation

$$n^F c_m^\gamma \mathbf{w}_\gamma = -D^\gamma \left(\frac{s^\gamma}{R\theta} \operatorname{grad} \mathcal{P} + \operatorname{grad} c_m^\gamma + z^\gamma \frac{c_m^\gamma}{R\theta} \operatorname{grad} \mathcal{E} \right) + n^F c_m^\gamma \mathbf{w}_F \quad (20)$$

describing the diffusion of the cations within the moving fluid. In the above relations, k^F is the *Darcy* permeability, γ^{FR} is the effective fluid weight, s^γ is the ion saturation ($s^\gamma = n^\gamma / n^F$), R denotes the universal gas constant, θ is the absolute *Kelvin* temperature, and $\mathcal{E}$ is the electrostatic force acting on one mole of positively charged ions. Note in passing that the electrostatic force $\mathcal{E}$ is a *Lagrange*an multiplier like $\mathcal{P}$, however, acting on the electroneutrality condition. Since it is assumed that there is no electrical current across the domain, the gradient of $\mathcal{E}$ may be obtained from the condition of a vanishing electrical current $\mathbf{i}$, cf., e.g., [29]:

$$\mathbf{i} = n^F (c_m^+ \mathbf{w}_+ - c_m^- \mathbf{w}_-) = \mathbf{0}. \quad (21)$$

After insertion of the ion diffusion velocities (20) and rearranging the resulting relation, the gradient of the electrostatic force $\mathcal{E}$ yields

$$\operatorname{grad} \mathcal{E} = -R\theta \left[\frac{s^+ D^+ - s^- D^- + D^L}{R\theta\, \varpi} (\operatorname{grad} \mathcal{P} - \rho^{FR}\, \mathbf{b}) - \frac{D^- - D^+ - 2D^L \left(\frac{2c_m - c_m^{fc}}{2c_m - c_m^{fc} + c_m^L} \right)}{\varpi} \operatorname{grad} c_m + \frac{D^- - D^L \left(\frac{2c_m - c_m^{fc}}{2c_m - c_m^{fc} + c_m^L} \right)}{\varpi} \operatorname{grad} c_m^{fc} \right]. \quad (22)$$

Therein, the abbreviation $D^L = c_m^{fc} k^F R\theta / (n^F \gamma^{FR})$ has been used and is interpreted as the diffusion coefficient of the liquid, while $\varpi = D^+ c_m + D^- (c_m - c_m^{fc}) + D^L c_m^{fc}$. Note that within the specimen, the electrical current originates from different sources which are not assumed to vanish individually. In particular, convection current occurs because of changes of the hydraulic as well as of the osmotic pressure (grad $\mathcal{P}$ and grad c_m), whereas diffusion current is caused by concentration differences (grad c_m). Both of these currents compete with the conduction current resulting from differences of the electrostatic force within the specimen (grad $\mathcal{E}$). For a more detailed explanation, the interested reader is referred to [30].

Now, the above equations can be inserted into each other to obtain a model for swelling phenomena with finite deformations. In particular, the gradient of the electrostatic force is inserted into the fluid flow and the ion diffusion equations. Thereafter, both equations are inserted into the corresponding balance relations to replace the variables $n^F \mathbf{w}_F$ and $n^F c_m \mathbf{w}_+$. Furthermore, the mechanical solid extra stress in Eq. (16) is replaced by the Neo-*Hooke*an law (18). Following this, a new and thermodynamically consistent formulation is derived with only three PDEs in the primary variables $\mathbf{u}_S$, p and c_m.

2.5.3 Electrochemical relations

For the above mentioned set of PDEs, initial and boundary conditions are needed. Particularly, the osmotic pressure and the cation concentration have to be initialised by non-zero initial values. Therefore, the well-known *Donnan* theory is used [8], which describes the interaction of large molecules with the ions of a salt dissolved in a solution. Inserting the electroneutrality condition (7) of the internal solution into the *Donnan* equation ($c_m^+ c_m^- = \bar{c}_m^+ \bar{c}_m^-$), it is possible to calculate the cation concentration and the osmotic pressure difference at the boundary. Thus,

$$\begin{aligned} c_m &= \sqrt{\bar{c}_m^2 + \tfrac{1}{4}(c_m^{fc})^2} + \tfrac{1}{2} c_m^{fc} \quad \text{and} \\ \Delta\pi &= p - \bar{p} = R\theta \left(\textstyle\sum_\gamma c_m^\gamma - \sum_\gamma \bar{c}_m^\gamma \right) \\ &= R\theta \, (2\, c_m - c_m^{fc} - 2\, \bar{c}_m), \end{aligned} \tag{23}$$

respectively, cf., e.g., [28,44]. Note that the osmotic pressure is obtained by the osmolarity difference of the internal and external solutions.

In Fig. 3, the different pressures inside and outside the material domain along with the corresponding pressure curve across the boundary are depicted. Therein, the internal pressure is the overall pressure p, i.e., $p = \mathcal{p} + \pi$, while the external pressure is the hydraulic pressure $\bar{p}$ plus the external osmotic pressure $\bar{\pi}$. Note that the internal and the external hydraulic pressures are equal. The excess pressure results from the fact that each solution has an individual osmotic pressure stemming from its own osmolarity ($\sum_\gamma c_m^\gamma$ and $\sum_\gamma \bar{c}_m^\gamma$). However, only the difference $\Delta\pi$ of the osmotic pressure, the pressure jump across the boundary, and not the ambient $\bar{\pi}$ is relevant at the boundary. It is important that both of the above Eq. (23) are only used for prescribed equilibrium states, i.e., as initial conditions and, as we assume that the boundary layer elements are immediately in equilibrium with the external solution, as boundary conditions. As was already mentioned, the values indicated by a bar denote the given values of the external solution. Already at this point, it can be recognised that this kind of boundary conditions need a special treatment.

3 Numerical implementation

The governing set of equations will be treated numerically within the framework of the FEM. For this purpose, the weak formulations of the PDEs will be derived in this section by the *Galerkin* procedure. In particular, the momentum balance (16) of the overall aggregate corresponding to the primary variable $\mathbf{u}_S$, the volume balance (14) of the overall fluid corresponding to the overall pressure p and the concentration balance (15) of the cations corresponding to the concentration c_m are multiplied by their respective test functions $\delta\mathbf{u}_S$, δp and δc_m and integrated by parts over the domain Ω via the divergence theorem. Finally, applying the *Gauß* theorem leads to the weak forms, cf. [2,11,13,46].

It is obvious from Eq. $(13)_2$ that the concentration of the fixed charges depends on the solid deformation ($c_m^{fc} = c_m^{fc}(\mathbf{u}_S)$). As a result, the boundary conditions also depend on $\mathbf{u}_S$, cf. (23). In order to include deformation-dependent boundary conditions for c_m^{fc} into the computation of a current time step, a first attempt might be to take the values of c_m^{fc} from the time step before. However, in an implicit time-integration scheme such as the backward-*Euler* scheme, this procedure includes an element of an explicit time integration into the numerical procedure, thus leading to enormous numerical instabilities, such as spurious oscillations. In particular, proceeding from the unconditionally stable implicit time-integration scheme (backward/implicit *Euler*), wherein the system of equations is solved by use of the variables computed within the current time and *Newton* step, i.e., within the residuum, the inclusion of c_m^{fc} from the time step before lets the whole algorithm react as if it would be an explicit scheme.

To illustrate the importance of including deformation-dependent values of c_m^{fc} at the boundary into the computation, a simple 1-d swelling example of hydrogel is considered, where the results of deformation-dependent c_m^{fc} at the boundary are compared to constant c_m^{fc}. Recall that, as was mentioned in the introduction, a purely 1-d simulation is numerically stable, since there are no gradients in a second spatial direction. The geometry and the parameters of the present example are basically the same as given in Sect. 4.1 and Table 1, where the salt concentration of the bathing solution is changed from 0.15 to 0.125 mol/l within 10 s. As one can see in Fig. 4, there is a distinct difference in the vertical displacement of the upper boundary if the concentration of the fixed charges c_m^{fc} at the domain boundary is taken as constant or deformation-dependent.

Proceeding from boundary conditions depending on $c_m^{fc}(\mathbf{u}_S)$ prescribes dependencies on both time and primary variables. Boundary conditions of this kind are also well known in the fields of modelling FSI, moving boundaries or free surfaces [9,41,42]. From the fluid-mechanical point of view, the conditions at the fluid boundary change with

Table 1 Material parameters used for the equilibrium test

$c^{fc}_{m0S} = 0.2$ meq/l	$n^S_{0S} = 0.25$
$\bar{c}_{m0} = 0.15$ mol/l	$\mu^S = 0.24$ N/mm^2
$c^L_m = 55.80$ mol/l	$\lambda^S = 0.02$ N/mm^2
$D^+ = 0.5 \times 10^{-3}$ mm^2/s	$\gamma^{FR} = 1 \times 10^{-5}$ N/mm^3
$D^- = 0.8 \times 10^{-3}$ mm^2/s	$k^F = 1.07 \times 10^{-8}$ mm/s
$R = 8.3144$ J/K mol	$\theta = 298$ K
$\epsilon = 1.0$	

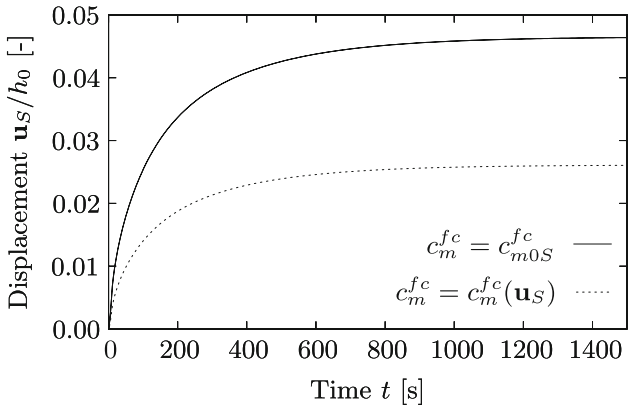

Fig. 4 Comparison of the vertical displacement of the upper node using boundary conditions with constant c^{fc}_m ($c^{fc}_m = c^{fc}_{m0S}$) and deformation dependent c^{fc}_m ($c^{fc}_m = c^{fc}_m(\mathbf{u}_S)$)

the deformation of the structure. For the solution of such problems, there are basically three different possibilities, cf. [18,42] or [19]: (1) simultaneous methods, (2) partitioned methods and (3) field-elimination methods. In the case of a simultaneous solution, both the fluid and the structure are solved simultaneously within one combined computational algorithm considering all physical properties, i.e., by use of a monolithic solution of the coupled problem. In contrast, applying the partitioned solution strategy, both parts, the structure and the fluid solution, are computed in an iterative manner (staggered scheme) using different specialised and effective algorithms by applying the solution of the one domain as a load onto the other. The third possibility, when all the governing equations concerning one component are eliminated such as describing the interaction between a fluid and a stiff solid structure, is usually avoided in the field of FSI [42].

In case of free surface flow problems, there is also an additional restriction needed to model moving boundaries. Depending on the basic choice of the setting, i.e., *Lagrange*an, *Euler*ian or arbitrary *Lagrange*an–*Euler*ian, different possibilities for the implementation of the additional condition are possible, cf., e.g., [38] for a review in *Euler*ian settings. Considering firstly the *Lagrange*an setting, which is also used in the present contribution, the governing equations are given such that the FE mesh moves with the free surface. For this formulation, [26] introduced additional primary variables maintaining the extra conditions at the free surface boundary. Later, [23,36,37] incorporated the boundary condition for the free surface into the *Lagrange*an weak form of the *Navier–Stokes* equation for single-phasic fluids. Considering secondly the *Euler*ian setting with a fixed mesh, as it is usually chosen in fluid mechanics, one proceeds from methods like the surface marker method to locate the boundary. Currently, the arbitrary *Lagrange*an–*Euler*ian (ALE) formulation is mostly used, where the boundary is described in an *Lagrange*an and the domain in an *Euler*ian setting, cf., e.g., [25,43].

Since multiphasic and multi-physical problems within the TPM generally result in a strongly linked system of volumetrically coupled PDEs, it is obvious that a simultaneous solution of the governing equations is necessary. Applying the above considerations made within the *Lagrange*an setting to the problem under consideration, two of the essential boundary conditions of the three PDEs will be imposed weakly. This is discussed in detail in the following section by incorporation of the boundary conditions via a penalty-like method into the weak formulation of the corresponding balance relation, cf. [24,47]. By use of this procedure, the boundary conditions are included into the residuum and computed within each *Newton* step. As a result, they always coincide with the current state of primary variables, thus overcoming the problem of spurious oscillations. Note in passing that, in this contribution, the weak imposition of *Dirichlet* boundary conditions is performed for multiple primary variables simultaneously.

3.1 Weak formulations

In the frame of the *Galerkin* procedure to obtain the weak form of the governing equations, this method is firstly applied to the volume balance (14) of the overall fluid. Thus,

$$\int_\Omega n^F \mathbf{w}_F \cdot \operatorname{grad} \delta p \, \mathrm{d}v - \int_\Omega \operatorname{div} (\mathbf{u}_S)'_S \, \delta p \, \mathrm{d}v = \int_{\Gamma_{\bar{q}}} \bar{q} \, \delta p \, \mathrm{d}a. \tag{24}$$

Therein, δp is the test function fulfilling the homogeneous *Dirichlet* boundary conditions, while the *Neumann* boundary condition $\bar{q}$ is the scalar value of fluid volume efflux over the boundary given by

$$\bar{q} = n^F \mathbf{w}_F \cdot \mathbf{n}, \tag{25}$$

where $\mathbf{n}$ denotes the outward-oriented unit surface normal. As depicted in Fig. 5, the entire boundary of the domain Ω corresponding to this PDE is denoted by Γ_F and is the

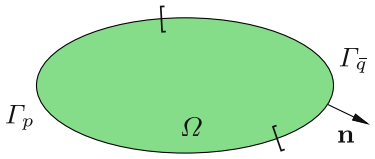

Fig. 5 Domain Ω with boundaries Γ_p and $\Gamma_{\bar{q}}$ for φ^F

set union of the *Dirichlet* boundary Γ_p and the *Neumann* boundary $\Gamma_{\bar{q}}$:

$$\Gamma_F = \Gamma_p \cup \Gamma_{\bar{q}}. \tag{26}$$

Proceeding from (24), the *Dirichlet* boundary conditions have to be fulfilled strongly. This implies that within the numerical procedure, the DOF have to fulfil prescribed values at the boundary. Because of the previously mentioned reasons, this procedure will be avoided and the *Dirichlet* boundary conditions will be imposed weakly.

Following this, the jump condition $(23)_2$ for the osmotic pressure at the boundary is rearranged to yield zero, multiplied by the test function δp, integrated over the surface where the overall pressure is applied and inserted into the weak form of the fluid volume balance:

$$\begin{aligned}&\int_\Omega n^F \mathbf{w}_F \cdot \operatorname{grad} \delta p \, \mathrm{d}v - \int_\Omega \operatorname{div} (\mathbf{u}_S)'_S \, \delta p \, \mathrm{d}v \\ &\quad + \int_{\Gamma_p} \epsilon \left[p - \bar{\mathcal{P}} - R\theta \, (2c_m - c_m^{fc} - 2\bar{c}_m) \right] \delta p \, \mathrm{d}a \\ &= \int_{\Gamma_{\bar{q}}} \bar{q} \, \delta p \, \mathrm{d}a. \end{aligned} \tag{27}$$

Therein, the third term on the left-hand side corresponds to the weak imposition of the *Dirichlet* boundary condition on Γ_p, where the parameter ϵ is a penalty parameter, which has to be chosen appropriately for the problem, i.e., as large as possible to reach a high accuracy, but also as low as possible to obtain convergence. Finally, the initial condition for the overall pressure p_0 is given by

$$p_0 = \Delta\pi_0 + \bar{\mathcal{P}}_0 = R\theta \, (2\, c_{m0} + c_{m0S}^{fc} - 2\, \bar{c}_{m0}) + \bar{\mathcal{P}}_0. \tag{28}$$

Concerning the cation concentration balance, the derivation of its standard weak form results in

$$\begin{aligned}&- \int_\Omega [\, n^F (c_m)'_S + c_m \operatorname{div} (\mathbf{u}_S)'_S \,] \, \delta c_m \, \mathrm{d}v \\ &+ \int_\Omega n^F c_m \mathbf{w}_+ \cdot \operatorname{grad} \delta c_m \, \mathrm{d}v \;=\; \int_{\Gamma_{\bar{j}}} \bar{j} \, \delta c \, \mathrm{d}a. \end{aligned} \tag{29}$$

Therein, δc_m is the corresponding test function and

$$\bar{j} = n^F c_m \mathbf{w}_+ \cdot \mathbf{n} \tag{30}$$

is the scalar value of the cation efflux over the *Neumann* boundary $\Gamma_{\bar{j}}$ of the domain Ω, where the entire boundary of Ω corresponding to the PDE of the cations is the set union

$$\Gamma_+ = \Gamma_c \cup \Gamma_{\bar{j}}. \tag{31}$$

Therein, Γ_c is the *Dirichlet* boundary, where usually the prescribed values of the cation concentration would have to be fulfilled strongly. But, as the concentration boundary condition is deformation-dependent, this boundary condition will also be included into the weak form as it has been done before for the volume balance. Thus, $(23)_1$ is rearranged to yield zero, multiplied by the test function δc_m and integrated over the *Dirichlet* surface Γ_c where the cation concentration is applied. Thereafter, the resulting expression is inserted into (29). This leads to the weak form of the cation concentration balance:

$$\begin{aligned}&- \int_\Omega [\, n^F (c_m)'_S + c_m \operatorname{div} (\mathbf{u}_S)'_S \,] \, \delta c_m \, \mathrm{d}v \\ &+ \int_\Omega n^F c_m \mathbf{w}_+ \cdot \operatorname{grad} \delta c_m \, \mathrm{d}v \\ &+ \int_{\Gamma_c} \epsilon \left[c_m - \sqrt{\bar{c}_m^2 + \tfrac{1}{2} (c_m^{fc})^2} - \tfrac{1}{4} c_m^{fc} \right] \delta c_m \, \mathrm{d}a \\ &= \int_{\Gamma_{\bar{j}}} \bar{j} \, \delta c \, \mathrm{d}a. \end{aligned} \tag{32}$$

Therein, the third term on the left-hand side is the weakly imposed *Dirichlet* boundary condition. Finally, the initial condition for the cation concentration c_{m0} is given by

$$c_{m0} = \sqrt{\bar{c}_{m0}^2 + \tfrac{1}{4} (c_{m0S}^{fc})^2} + \tfrac{1}{2} c_{m0S}^{fc}. \tag{33}$$

Since there is no need for a special treatment of the displacement boundary conditions, the weak form of the momentum balance, i.e.,

$$\begin{aligned}&\int_\Omega (\mathbf{T}^S_{E\,mech.} - p\, \mathbf{I}) \cdot \operatorname{grad} \delta \mathbf{u}_S \, \mathrm{d}v \\ &- \int_\Omega (\rho^S + \rho^F) \, \mathbf{b} \cdot \delta \mathbf{u}_S \, \mathrm{d}v = \int_{\Gamma_{\mathbf{t}}} \bar{\mathbf{t}} \cdot \delta \mathbf{u}_S \, \mathrm{d}a \end{aligned} \tag{34}$$

did not change and keeps its well-known form.

As usual, the computation starts from a stress-free and, therefore, from an undeformed reference state. Following this, the referential extra stress is set to zero:

$$\mathbf{T}^S_{E\,mech.0} = \mathbf{0}. \tag{35}$$

During loading, the traction boundary conditions are given by

$$\bar{\mathbf{t}} = (\mathbf{T}^S_{E\,mech.} - p\, \mathbf{I})\, \mathbf{n}, \tag{36}$$

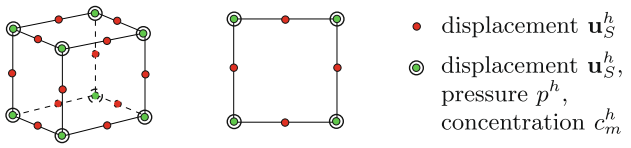

Fig. 6 Spatial discretisation using extended *Taylor-Hood* elements

where the overall boundary corresponding to this balance relation is the set union

$$\Gamma_S = \Gamma_{\mathbf{u}} + \Gamma_{\mathbf{t}} \tag{37}$$

composed of the *Dirichlet* and *Neumann* parts, $\Gamma_{\mathbf{u}}$ and $\Gamma_{\mathbf{t}}$, respectively.

3.2 Discretisation

The values of the degrees of freedom are obtained by solving the set (27), (32) and (34) of weak forms by the mixed finite element scheme. Note that one has to use the mixed FEM, since there are further primary variables in addition to the solid displacement $\mathbf{u}_S$. Concerning the model proposed in this contribution, these are the overall pore-fluid pressure p and the cation concentration c_m. The choice of convergent approximation spaces in mixed methods is by no means automatic, as in mixed methods the patch test or, more general, the inf-sup condition (*Babuška-Brezzi* condition) has to be fulfilled, cf. [7,45]. Both conditions are satisfied if the approximation of the displacement is chosen one order higher than those of the pressure and the concentration in order to avoid spurious modes in the pressure and the concentration fields. Therefore, as depicted in Fig. 6, the spatial discretisation proceeds from a quadratic approximation of the solid displacement and linear approximations for the overall pore-fluid pressure and the cation concentration (Q2P1C1). This type of mixed finite elements is known as extended *Taylor-Hood* elements. The discretisation in the time domain is carried out by the unconditionally stable implicit *Euler* algorithm. The whole model is implemented into the FE tool PANDAS[1], which has been especially designed for the solution of volumetrically coupled problems.

4 Numerical examples

4.1 Chemical equilibrium test

To validate the stabilised model, a 2-d free swelling experiment under 1-d loading conditions is carried out using hydrogel as the swelling material. In fact, the numerical experiment consists of keeping the sample in its initial state by applying equilibrium boundary conditions. A sketch of the geometry with the size $0.02 \times 0.5\,\mathrm{mm}^2$ is given in Fig. 7. This geometry is discretised by 1×30 quadrilateral extended *Taylor-Hood* elements. Furthermore, the boundary conditions consist of hindering the solid skeleton displacements (*Dirichlet*, $\Gamma_{\mathbf{u}}$) at the lower, the left and the right boundaries in the direction perpendicular to the surface and, at the same boundaries, hindering the fluid flow and the ion diffusion (*Neumann*, $\Gamma_{\bar{q}}$ and $\Gamma_{\bar{j}}$). The equilibrium conditions for both the osmotic pressure and the cation concentration (*Dirichlet*, Γ_p and Γ_c) are applied at the upper edge by keeping the concentration constant, cf. Fig. 7. The material parameters used for the computation are listed in Table 1. Considering the result of this computation, one would expect that nothing happens and everything stays at its initial state.

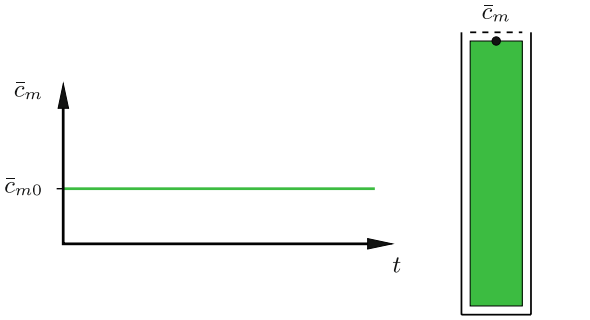

Fig. 7 *Left*: Chemical loading, the concentration of the external solution is kept constant. *Right*: Sketch of the geometry with the observed upper node

In the first computation, the weak forms are evaluated in their standard representations without the weakly imposed *Dirichlet* boundary conditions, i.e., without the third term on the left-hand side of Eqs. (27) and (32). With this method, the boundary conditions have to be evaluated separately by relations (23) using the value of the internal variable c_m^{fc} from the last time step. As one can see in the upper diagram of Fig. 8, the computation starts to oscillate apparently around the equilibrium state after a while, even though the unconditionally stable implicit *Euler*ian time-integration scheme is used. The reason for these oscillations result from small numerical errors made at each time step by using c_m^{fc} from the time step before. Although the value of c_m^{fc} is only used for the boundary conditions, the whole code behaves by this procedure as if it would be an explicit scheme. In contrast, the result obtained using the weak forms (27) and (32) including the weakly fulfilled boundary conditions is stable. As expected, the vertical displacement of the observed node on the upper boundary is zero and the specimen persists in its initial state. The reason is that the concentration and osmotic pressure applied at the boundary by the weakly imposed representation are always in line with the current deformation and therefore with the current concentration of the fixed charges. Note that with $\epsilon = 1.0$, there is no distinct weighting

[1] **P**orous media **A**daptive **N**onlinear finite element solver based on **D**ifferential **A**lgebraic **S**ystems (http://www.get-pandas.com).

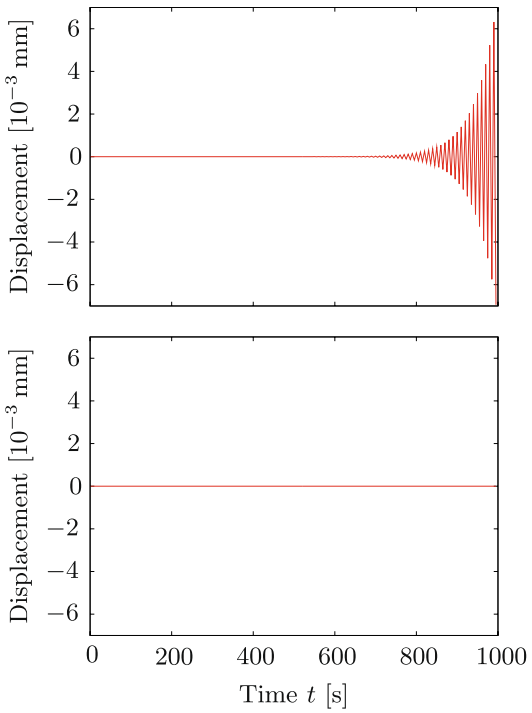

Fig. 8 Vertical displacement of node A. Strongly fulfilled boundary conditions in the upper figure versus weakly fulfilled boundary conditions in the lower one

of the boundary terms for this initial boundary-value problem (IBVP).

4.2 2-d swelling example

The aim of this section is to show the capability of the introduced model and its implementation by a 2-d computation of a free swelling experiment exhibiting finite deformations. Such an experiment has been carried out by the group of Jacques Huyghe at the Biomedical Engineering department of the Eindhoven University of Technology. In this experiment, a soot-coloured cylindrical block was cut out of a hydrogel stick made in a test-tube and was thereafter immediately placed in a sodium chloride solution. While placing the specimen in this solution, all its surfaces have been in contact with the new bath. Therefore, the swelling procedure was initiated at all surfaces at once. The concentration in the new solution compared to the previous one was so low and, as a result, the osmotic pressure was so high that the hydrogel cylinder did undergo an enormous volumetric change until its final equilibrium state, cf. Fig. 10.

To simulate this experiment, a rectangular cross section is discretised under plane-strain conditions by use of symmetry conditions. In particular, half of the geometry, namely, an area of $1.1 \times 1.0\,\mathrm{mm}^2$ is meshed by 22×20 eight-noded extended *Taylor-Hood* elements. During the computation, the chemically uncharged hydrogel is firstly equilibrated in

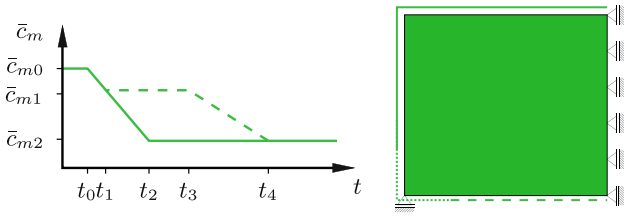

Fig. 9 Chemical loading and geometry of the 2-d free swelling simulation. The *solid* and the *dashed* concentration curves on the left side belong to the respective boundaries on the right side. The *dotted line* at the bottom's left corner of the right-hand picture denotes the interval with the transition zone from the value of the solid concentration curve to the dashed one

a bathing solution with the initial concentration $\bar{c}_{m0}$. This is necessary in order to transform the hydrogel from a fictitious non-loaded reference configuration in the sense of a natural state at $t = t_0$ towards a pre-swollen initial configuration. Note in passing that in any real experiment, there is no uncharged configuration, since swelling materials are always somehow in a swollen state. In the fictitious non-loaded reference configuration, there is neither a solid stress ($\mathbf{T}^S_{E\,mech.0} = 0$) nor an osmotic pressure ($\pi_0 = 0$). To avoid numerical problems during initial loading, the initial osmotic pressure is applied slowly by increasing the referential concentration of the fixed charges from 0 to the prescribed value c^{fc}_{m0S} over time.

After a certain time of computation, an equilibrium state is reached defined as the "initial configuration" at which the initial osmotic pressure π^*_0, the initial concentration c^*_{m0} and the initial purely mechanical solid extra stress $\mathbf{T}^{S\,*}_{E\,mech.0}$ fits the deformation $(\det \mathbf{F}_S)^*_{0S}$ through the balance and constitutive equations. Note that the quantities corresponding to the deformed initial configuration (equilibrium state) are denoted by $(\cdot)^*_{0S}$.

The boundary conditions applied to this geometry are depicted in Fig. 9. In particular, on the right-hand side, the symmetry conditions are applied (hindered horizontal movement, undrained) and the bottom left node is fixed in vertical direction. The intention of this displacement constraints is to mimic the contact situation of the actual experiment. Compared to this, the concentration and osmotic pressure boundary conditions are quite complex. At the beginning of the simulation, after having found the initial state, the concentration is firstly changed at all boundaries. This is the time period, where the specimen is placed in the new solution. As one can see from the sequence of pictures of Fig. 10, there is an irregular shape at the beginning of the deformation. The reason for this initial irregularities is negative osmosis, cf. [22], which means that there is an initial inflow of fluid into the specimen and, at the same time, a flow of interstitial fluid from the inner region of the specimen towards its boundary. This effect leads to an initial shrinking of the inner part of

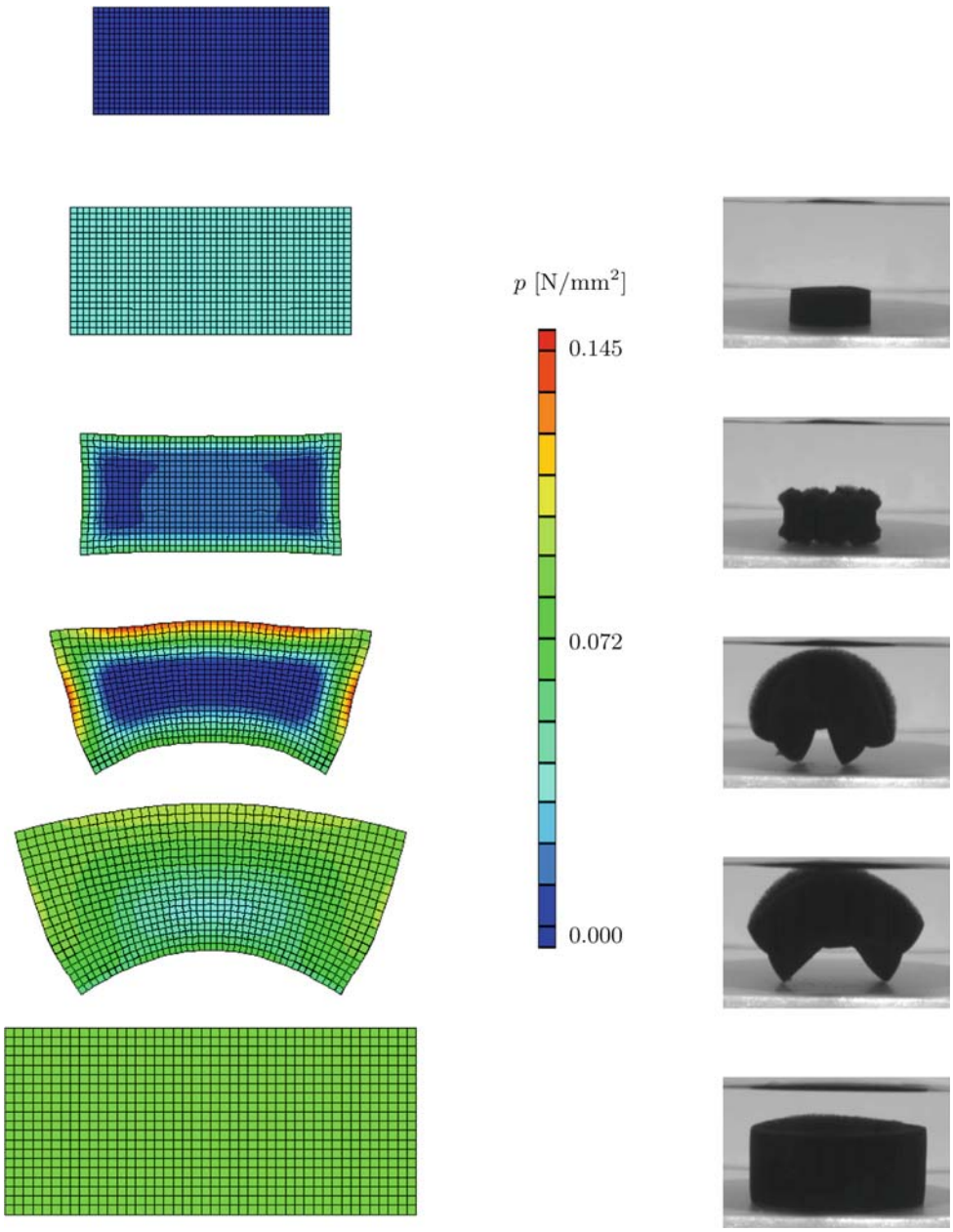

Fig. 10 Qualitative comparison between the numerical simulation and the experiment with a soot-coloured hydrogel disc carried out by the group of J. Huyghe. The most upper geometry on the *left* is the stress-free and non-swollen reference configuration. Beneath, there is the pre-swollen initial state. The following *contour plots* show the deformation and the overall pressure up to the final equilibrium state

the hydrogel, while the circumferential edges are already swelling. The resulting discrepancy in the deformation is the cause of the frayed border of the soot-coloured cylinder. Negative osmosis happens only if $c_{0S}^{fc*} \ll \bar{c}_{m0}^{*}$. A closer look at the equation

$$\Delta\pi = 2\,R\theta\left[\sqrt{\bar{c}_m^2 + \tfrac{1}{4}\,(c_m^{fc})^2} - \bar{c}_m\right] \tag{38}$$

obtained by inserting $(23)_1$ in $(23)_2$ reveals that the term $(c_m^{fc})^2$ is less relevant in this case, and the osmotic pressure decreases initially with the faster decreasing $\bar{c}_m^2$ such that the fluid from the inner regions flows towards the outer ones. After this period, the concentration is only changed at the top and at the circumferential boundary. Note that there is an additional boundary interval at the bottom left corner, cf. Fig. 9 right, with a length of $0.3+0.3$ mm for a seamless transition from the circumferential concentration to the bottom concentration. This transition has been introduced to avoid numerical problems resulting from discontinuous boundary conditions at the corner.

Concerning the numerical simulation prior to the actual swelling process, the specimen is equilibrated for a period of $t_0 = 7{,}000$ s in a $c_{m0} = 4.1$ molar NaCl solution, where c_{m0S}^{fc} is increased from 0 to 0.8 meq/l within the first 4,000 s. After equilibrium is obtained, the initial configuration is reached, and the hydrogel is placed in the new NaCl bathing solution.

Table 2 Material parameters used for the simulation of the 2-d free swelling experiment

$c^{fc}_{m0S} = 0.8$ meq/l	$n^S_{0S} = 0.25$
$\bar{c}_{m0} = 4.10$ mol/l	$\mu^S = 0.12$ N/mm^2
$c^L_m = 55.80$ mol/l	$\lambda^S = 0.02$ N/mm^2
$D^+ = 0.5 \times 10^{-3}$ mm^2/s	$\gamma_{FR} = 1 \times 10^{-5}$ N/mm^3
$D^- = 0.8 \times 10^{-3}$ mm^2/s	$k^F = 1.07 \times 10^{-8}$ mm/s
$R = 8.3144$ J/K mol	$\theta = 298$ K
$c^{fc*}_{m0S} = 0.51$ meq/l	$n^{S*}_{0S} = 0.18$
$\epsilon = 40.0$	

Following this, the external salt concentration is decreased at all boundaries from $\bar{c}_{m0} = 4.1$ mol/l to $\bar{c}_{m1} = 2.7$ mol/l until $t_1 = 7{,}080$ s. Thereafter, only the boundaries denoted by the solid line are exposed to the solution. Here, the concentration is further decreased to $\bar{c}_{m2} = 0.3$ mol/l until $t_2 = 7{,}220$ s, while the concentration at the bottom is kept constant. At $t_3 = 8{,}000$ s, the bottom of the hydrogel gets in contact with the bathing solution as well. Therefore, $\bar{c}_{m1}$ is decreased here to $\bar{c}_{m2} = 0.3$ mol/l until $t_4 = 10{,}000$ s.

For the present 2-d simulation, the weighting factor ϵ has been chosen to 40.0. Therewith, the computation of the IBVP is stable and exhibits a good convergence. For convenience, all material parameters used for the simulation are summarised in Table 2. Note that it is well known that for such high concentrations, osmotic and activity coefficients should come into play. But since the concentrations vary during the simulation on a very large range, these coefficients would depend on the concentrations. Since the main attention within this contribution was on the weakly imposed *Dirichlet* boundary conditions, these factors have been omitted here.

In Fig. 10, the simulation results on the left-hand side are compared with the experiment on the right-hand side. Besides the comparison of the deformation, the contour plots show the development of the overall fluid pressure within the material. The top picture at the left depicts the stress-free reference configuration ($t = 0$ s), where there is no deformation and no osmotic pressure. Beneath, one can see the calculated initial configuration ($t_0 = 7{,}000$ s) after having increased c^{fc}_{0S} from 0 to its full amount and having reached equilibrium. This is a swollen state, i.e., there is an osmotic pressure and a deformation. The third line shows the phase of the negative osmosis ($t = 7{,}107$ s), during which the hydrogel shrinks initially in its inner region. Thereafter, the state with the highest bending is shown ($t = 7{,}224$ s). The subsequent pictures present how the final equilibrium state is reached ($t = 7{,}650$ s and $t = 11{,}000$ s). Note that the cross-sectional area of the specimen at the end of the simulation is approximately 2.2 times the area of the (calculated) initial state.

5 Conclusions

In this contribution, a consistent model for swelling materials like charged, hydrated porous media based on the well-founded TPM has been derived. Moreover, finite deformations of the solid skeleton have been considered by the Neo-*Hooke*an model presented by [12] such that swelling experiments with finite volumetric deformations can be simulated accurately. The advantage of this model is that only three primary variables are necessary to model swelling processes, namely, the solid displacement $\mathbf{u}_S$, the overall pore-fluid pressure p and the cation concentration c_m. This reduction of the degrees of freedom results not only in a numerically effective model, but also in deformation-dependent boundary conditions which have to be treated properly.

Therefore, we proposed in the present contribution to fulfil the *Dirichlet* boundary conditions for the osmotic pressure and the cation concentration weakly by incorporation of the corresponding conditions into the weak forms of the respective balance relations. Treating the boundary conditions by this procedure, the numerical simulations remain stable.

Finally, in the last section, the numerical treatment of the model has been validated by a 2-d simulation of a 1-d swelling experiment. One could see that fulfilling the *Dirichlet* boundary conditions strongly leads to oscillations while the simulation with the weakly fulfilled boundary conditions yields stable results. The capability and the stability of the implemented code has been finally exhibited by a real free-swelling simulation with finite deformations, and the results have been compared qualitatively with an experiment.

Acknowledgments We thank the German Research Foundation (DFG) for funding the Dutch-German research unit "Multiscale Methods in Computational Mechanics" (MMCM, http://www.ibb.uni-stuttgart.de/for_509). This work has been developed within the sub-project IV-D "Theoretical and Numerical Investigations of Swelling Phenomena of Hydrated Porous Media" (http://www.mechbau.uni-stuttgart.de/ls2).

References

1. Acartürk A, Ehlers W, Abbas I (2004) Modelling of swelling phenomena in charged hydrated porous media. PAMM 4:296–297
2. Bathe K-J (1996) Finite element procedures, 2nd edn. Prentice-Hall, Englewood Cliffs
3. de Boer R (2000) Theory of porous media. Springer, Berlin
4. de Boer R, Ehlers W (1986) Theorie der Mehrkomponentenkontinua mit Anwendungen auf bodenmechanische Probleme. Forschungsberichte aus dem Fachbereich Bauwesen Heft 40, Universität-GH-Essen
5. Bowen RM (1976) Theory of mixtures. In: Eringen AC (ed) Continuum physics, vol III, mixtures and EM field theories. Academic Press, London pp 1–127

6. Bowen RM (1980) Incompressible porous media models by use of the theory of mixtures. Int J Eng Sci 18:1129–1148
7. Chapelle D, Bathe KJ (1993) The inf-sup test. Comput Struct 47:537–545
8. Donnan FG (1911) Theorie der Membrangleichgewichte und Membranpotentiale bei Vorhandensein von nicht dialysierenden Elektrolyten. Ein Beitrag zur physikalisch-chemischen Physiologie. Zeitschrift für Elektrochemie und Angewandte Physikalische Chemie 17:572–581
9. Dowell EH, Hall KC (2001) Modeling of fluid–structure interaction. Ann Rev Fluid Mech 33:445–490
10. Ehlers W (1989) Poröse Medien—ein kontinuumsmechanisches Modell auf der Basis der Mischungstheorie. Forschungsberichte aus dem Fachbereich Bauwesen, Heft 47, Universität-GH-Essen
11. Ehlers W (2002) Foundations of multiphasic and porous materials. In: Ehlers W, Bluhm J (eds) Porous media: theory, experiments and numerical applications. Springer, Berlin pp 3–86
12. Ehlers W, Eipper G (1999) Finite elastic deformations in liquid-saturated and empty porous solids. Transp Porous Media 34: 179–191
13. Ehlers W, Ellsiepen P (2001) Theoretical and numerical methods in environmental continuum mechanics based on the Theory of Porous Media. In: Schrefler BA (ed) Environmental geomechanics. Springer, Wien, CISM Courses and Lectures No. 417, pp 1–81
14. Ehlers W, Karajan N, Markert B (2006) A porous media model describing the inhomogeneous behaviour of the human intervertebral disc. Materialwissenschaften und Wekstofftechnik 37:546–551
15. Ehlers W, Karajan N, Markert B (2008) An extended biphasic model for charged hydrated tissues with application to the intervertebral disc. Biomech Model Mechanobiol. doi:10.1007/s10237-008-0129-y
16. Ehlers W, Markert B, Acartürk A (2005a) Swelling phenomena of hydrated porous materials. In: Abousleiman YN, Cheng AH-D, Ulm FJ (eds) Poromechanics III, Proceedings of the 3rd Biot Conference on Poromechanics. Balkema, Leiden pp 781–786
17. Ehlers W, Markert B, Karajan N, Acartürk A (2005b) A coupled FE analysis of the intervertebral disc based on a multiphasic TPM formulation. In: Holzapfel GA, Ogden RW (eds) IUTAM symposium on mechanics of biological tissue. Springer, Wien pp 373–386
18. Felippa CA, Park KC (1980) Staggered transient analysis procedures for coupled mechanical systems: formulation. Comput Methods Appl Mech Eng 24:61–111
19. Felippa CA, Park KC, Farhat C (2001) Partitioned analysis of coupled mechanical systems. Comput Methods Appl Mech Eng 190:3247–3270
20. Frijns AJH, Huyghe JM, Janssen JD (1997) A validation of the quadriphasic mixture theory for intervertebral disc tissue. Int J Eng Sci 35:1419–1429
21. Frijns AJH, Huyghe JM, Kaasschieter EF, Wijlaars MW (2003) Numerical simulation of deformations and electrical potentials in a cartilage substitute. Biorheology 40:123–131
22. Gu WY, Lai WM, Mow VC (1997) A triphasic analysis of negative osmotic flows through charged hydrated soft tissues. J Biomech 30:71–78
23. Hansbo P (1995) Lagrangian incompressible flow computations in three dimensions by use of space-time finite elements. Int J Numer Methods Fluids 20:989–1001
24. Hansbo P, Hermansson J (2003) Nitsche's method for coupling non-matching meshes in fluid-structure vibration problems. Comput Mech 32:134–139
25. Hirt CW, Amsden AA, Cook JL (1974) An arbitrary Lagrangian-Eulerian computing method for all flow speeds. J Comput Phys 14:227–253
26. Hirt CW, Cook JL, Butler TD (1970) A Lagrangian method for calculating the dynamics of an incompressible fluid with free surface. J Comput Phys 5:103–124
27. Huyghe JM, Janssen JD (1997) Quadriphasic mechanics of swelling incompressible porous media. Int J Eng Sci 35:793–802
28. Kaasschieter EF, Frijns AJH, Huyghe JMRJ (2003) Mixed finite element modelling of cartilaginous tissues. Math Comput Simul 61:549–560
29. Lai WM, Hou JS, Mow VC (1991) A triphasic theory for the swelling and deformation behaviours of articular cartilage. ASME J Biomech Eng 113:245–258
30. Lai WM, Mow VC, Sun DD, Ateshian GA (2000) On the electric potentials inside a charged soft hydrated biological tissue: Streaming potential vs. diffusion potential. ASME J Biomech Eng 122:336–346
31. Lanir Y (1987) Biorheology and fluidflux in swelling tissues. I. Bicomponent theory for small deformations, including concentration effects. Biorheology 24:173–187
32. van Loon R, Huyghe JM, Wijlaars MW, Baaijens FPT (2003) 3D FE implementation of an incompressible quariphasic mixture model. Int J Numer Methods Eng 57:1243–1258
33. Mow VC, Ateshian GA, Lai WM, Gu WY (1998) Effects of fixed charges on the stress-relaxation behavior of hydrated soft tissues in a confined compression problem. Int J Solids Struct 35:4945–4962
34. Mow VC, Kuei SC, Lai WM, Armstrong CG (1980) Biphasic creep and relaxation of articular cartilage in compression: theory and experiments. ASME J Biomech Eng 102:73–84
35. Mow VC, Ratcliffe A (1997) Structure and function of articular cartilage and meniscus. In: Mow VC, Hayes WC (eds) Basic orthopaedic biomechanics, 2nd edn. Lippincott-Raven, Philadelphia, pp 113–176
36. Radovitzky R, Ortiz M (1998) Lagrangian finite element analysis of newtonian fluid flows. Int J Numer Methods Eng 43:607–619
37. Ramaswamy B, Kawahara M (1987) Lagrangian finite element analysis applied to viscous free surface fluid flow. Int J Numer Methods Fluids 7:953–984
38. Scardovelli R, Zaleski S (1999) Direct numerical simulation of free-surface and interfacial flow. Ann Rev Fluid Mech 31:567–603
39. Snijders H, Huyghe JM, Janssen JD (1995) Triphasic finite element model for swelling porous media. Int J Numer Methods Fluids 20:1039–1046
40. Sun DN, Gu WY, Guo XE, Mow WMLVC (1999) A mixed finite element formulation of triphasic mechano-electrochemical theory for charged, hydrated biological soft tissues. Int J Numer Methods Eng 45:1375–1402
41. Tezduyar TE (2001) Finite element methods for flow problems with moving boundaries and interfaces. Arch Comput Methods Eng 8:83–130
42. Wall WA (1999) Fluid-Struktur-Interaktion mit stabilisierten Finiten Elementen. Dissertation, Institut für Baustatik, Universität Stuttgart
43. Wall WA, Genkinger S, Ramm E (2007) A strong coupling partitioned approach for fluid–structure interaction with free surfaces. Comput Fluids 36:169–183
44. Wilson W, van Donkelaar CC, Huyghe JM (2005) A comparison between mechano-electrochemical and biphasic swelling theories for soft hydrated tissue. ASME J Biomech Eng 127:158–165
45. Zienkiewicz OC, Qu S, Taylor RL, Nakazawa S (1986) The patch test for mixed formulations. Int J Numer Methods Eng 23: 1873–1883
46. Zienkiewicz OC, Taylor RL (2000) The finite element method, vol 1, 5th edn. Butterworth-Heinemann, Oxford
47. Zienkiewicz OC, Taylor RL, Sherwin SJ, Peiró J (2003) On discontinuous galerkin methods. Int J Numer Methods Eng 58:1119–1148